782–791 *Nucleic Acids Research, 2018, Vol. 46, No. 2* *Published online 6 December 2017*
doi: 10.1093/nar/gkx1171

Influence of thermodynamically unfavorable secondary structures on DNA hybridization kinetics

Hiroaki Hata, Tetsuro Kitajima and Akira Suyama*

Department of Life Sciences and Institute of Physics, The University of Tokyo, 3-8-1 Komaba, Meguro-ku, Tokyo 153-8902, Japan

Received March 18, 2017; Revised October 31, 2017; Editorial Decision November 08, 2017; Accepted December 04, 2017

ABSTRACT

Nucleic acid secondary structure plays an important role in nucleic acid–nucleic acid recognition/hybridization processes, and is also a vital consideration in DNA nanotechnology. Although the influence of stable secondary structures on hybridization kinetics has been characterized, unstable secondary structures, which show positive ΔG° with self-folding, can also form, and their effects have not been systematically investigated. Such thermodynamically unfavorable secondary structures should not be ignored in DNA hybridization kinetics, especially under isothermal conditions. Here, we report that positive ΔG° secondary structures can change the hybridization rate by two-orders of magnitude, despite the fact that their hybridization obeyed second-order reaction kinetics. The temperature dependence of hybridization rates showed non-Arrhenius behavior; thus, their hybridization is considered to be nucleation limited. We derived a model describing how ΔG° positive secondary structures affect hybridization kinetics in stopped-flow experiments with 47 pairs of oligonucleotides. The calculated hybridization rates, which were based on the model, quantitatively agreed with the experimental rate constant.

INTRODUCTION

An oligonucleotide strand binds to its complementary strand and forms a double helical structure, according to the Watson–Crick rules for base-pairing (1). Many important techniques used in biology utilize duplex formation or hybridization (2–5). The kinetics of oligonucleotide hybridization has been investigated since the 1960s (6–8). Earlier researchers proposed the nucleation-zipper model, consistent with their kinetic experiments (3,9). Based on this classical model, researchers later investigated the quantitative relationship between sequence properties and hybridization kinetics (10–12). However, compared with knowledge of the thermodynamics of DNA hybridization (13–15), our understanding of its kinetics is limited (16), and the prediction of hybridization rates from base sequences is still difficult.

Influences of secondary structure on the kinetic properties of hybridization have been investigated by many researchers (17–23). However, these studies focused only on sequences with stable secondary structures, which show a negative standard Gibbs free energy change (ΔG°) for secondary structure formation. There are also sequences with unstable secondary structures, which show a positive ΔG° ($|\Delta H^\circ| < |T\Delta S^\circ|$, $\Delta H^\circ < 0$, and $\Delta S^\circ < 0$, in Gibbs free energy calculation). Although such structures are thermodynamically unfavorable, they exist at almost the same concentration as the unstructured coil when the absolute value of ΔG° is very small. Thus, positive ΔG° secondary structures should no longer be ignored in hybridization kinetics, especially under isothermal conditions involved in numerous biosensor techniques and recent DNA network systems (24–28). Nevertheless, to our knowledge, influences of positive ΔG° secondary structures on hybridization kinetics have not been systematically investigated.

In this study, we characterized effects of positive ΔG° secondary structures on DNA hybridization kinetics. The hybridization kinetics for 47 pairs of 23-mer oligonucleotides was measured using stopped-flow fluorescence spectroscopy at different temperatures, and their secondary structures and duplex stabilities were studied by thermal melting. The observed hybridization kinetics was significantly dependent on the base sequence, and the rate constant varied by more than two orders of magnitude among sequences with no ΔG° negative secondary structures. The rate constant tended to decrease with the probability of intramolecular base pairing of positive ΔG° secondary structures. Their hybridization obeyed second-order reaction kinetics, and the temperature dependence of the rate constant showed non-Arrhenius behavior. Therefore, their hybridization must be nucleation limited, and so the reaction model presented by previous researchers to explain the effects of stable secondary structures on hybridization kinetics (a rate-limiting process based on destruction of secondary structure) was found not to be applicable in cases of

*To whom correspondence should be addressed. Tel +81 3 5454 6528; Fax: +81 3 5454 6528; Email: suyama@dna.c.u-tokyo.ac.jp

Table 1. List of DNA sequences used in this study, ΔG° (kcal/mol) values[a], ΔF^* values[b], second-order rate constants and experimental duplex melting temperatures

No.	Sequence	ΔG° (kcal/mol)		ΔF^* (a.u.)		k_{app}	T_m
		A strand	B strand	A strand	B strand	(10^5 $M^{-1}s^{-1}$)	(°C)
0	GCCCACACTCTTACTTATCGACT	2.2	1.7	1.12 ± 0.01	1.32 ± 0.01	35 ± 2	61.5
1	AGAGGCTTATAACTGTGTCGGGT	1.6	1.8	1.59 ± 0.02	1.30 ± 0.01	21.0 ± 0.7	63.0
2	TGTTCTAAGATTATCCTCCCGCC	1.8	1.7	1.410 ± 0.005	1.7 ± 0.2	22.1 ± 0.7	62.0
3	GGCGGCTATAACAATTTCATCCA	1.8	1.4	1.49 ± 0.01	2.26 ± 0.02	28 ± 2	63.5
4	TAGCCCAGTGATTTATGACATGC	1.5	1.4	3.2 ± 0.1	3.9 ± 0.1	4.3 ± 0.1	64.5
5	GCATCTACACTCAATACCCAGCC	1.4	1.4	1.841 ± 0.009	1.310 ± 0.002	43 ± 2	62.5
6	GCCCGTACTGTTGAGATTATGGT	0.96	1.8	1.9 ± 0.2	1.82 ± 0.04	9.2 ± 0.4	64.5
7	GCACCTCCAAATAAAAACTCCGC	1.6	0.94	1.10 ± 0.09	1.32 ± 0.02	48 ± 4	64.5
8	AGATCAGAGATAGTTACGCCGCA	1.2	1.2	1.68 ± 0.03	1.39 ± 0.09	12.5 ± 0.5	66.0
9	TATGTTCCTTACCCCGTTTACCA	1.3	0.96	1.4 ± 0.2	0.7 ± 0.3	7.3 ± 0.1	62.0
10	TAGCCAACTCTAAATAACGGACG	1.1	1.1	1.43 ± 0.01	1.54 ± 0.02	10.2 ± 0.2	63.5
11	GAAGGAATGTTAAAATCGTCGCG	1.0	1.0	1.47 ± 0.04	1.38 ± 0.03	7.7 ± 0.2	64.0
12	TTTGTTTTCCTTATGAGCCAGCC	1.2	0.94	1.18 ± 0.09	0.8 ± 0.6	14.3 ± 0.5	62.5
13	GCCCCGATATCTATTTTAGGACG	1.0	1.0	4.1 ± 0.3	2.3 ± 0.1	13.5 ± 0.8	62.5
14	CGCAGGAGAGTTAAACGAAAGCA	1.0	0.99	1.23 ± 0.09	1.0 ± 0.6	1.038 ± 0.009	64.5
15	GGCTCTATACGATTAAACTCCCC	1.2	0.76	1.66 ± 0.08	1.78 ± 0.05	15.5 ± 0.6	61.5
16	CATCTGAACGAGTAAGGACCCCA	1.2	0.76	1.84 ± 0.02	3.5 ± 0.2	12.1 ± 0.2	64.5
17	CGTCTATTGCTTGTCACTTCCCC	0.96	0.86	2.9 ± 0.1	2.1 ± 0.4	5.23 ± 0.04	65.5
18	AGTCCTTGGTTATCATTCCCTCT	0.85	0.93	1.55 ± 0.01	1.89 ± 0.03	10.5 ± 0.5	61.5
19	GGTCTCAGCTAATTTCACACAGA	0.85	0.85	1.21 ± 0.07	1.419 ± 0.009	6.3 ± 0.2	62.5
20	TGGGGGGCATAAAACGATACTAG	0.6	1.1	1.53 ± 0.01	1.30 ± 0.06	4.7 ± 0.08*	61.5
21	TGCTCACTTACATTACGTCCATG	0.93	0.7	3.7 ± 0.2	2.34 ± 0.07	7.0 ± 0.2	63.0
22	ACCCTTTATCCTGTAACTTCCGC	0.94	0.68	1.38 ± 0.08	1.213 ± 0.003	26 ± 2	63.0
23	GCCTAGTGAAACCGTAAGTGCAT	0.91	0.68	2.4 ± 0.1	3.3 ± 0.7	1.73 ± 0.03	65.0
24	TCAGCACTCTACTTGACGGACTT	0.74	0.82	2.13 ± 0.06	1.75 ± 0.02	0.874 ± 0.007	65.5
25	AGGTTAGGATTTGTCGGGAGATG	−0.049	1.3	1.52 ± 0.08	1.0 ± 0.2	31 ± 3	63.0
26	GTCCCGGAAAATACTATGAGACC	0.83	0.36	1.80 ± 0.06	2.9 ± 0.3	0.368 ± 0.003	61.5
27	GGCGCTTAAATCATCTTTCATCG	0.73	0.45	1.92 ± 0.03	5.93 ± 0.03	5.9 ± 0.2	64.5
28	CCGTCGTGTTATTAAAGACCCCT	0.15	0.62	1.94 ± 0.03	2.110 ± 0.008	0.759 ± 0.005	62.5
29	GAGTCAATCGAGTTTACGTGGCG	0.34	0.43	1.78 ± 0.07	1.88 ± 0.01	0.488 ± 0.006	65.0
30	TTCGGTTCTCTCCAAAAAAAGCA	0.85	−0.18	2.74 ± 0.09	4.16 ± 0.03	2.17 ± 0.03	62.0
31	TGGCACTTATAGCTGTCGGAAGA	−0.15	0.71	2.94 ± 0.08	2.3 ± 0.2	1.58 ± 0.01	63.5
32	GAGTCCGCAAAAATATAGGAGGC	−0.083	0.38	1.43 ± 0.06	1.68 ± 0.02	22.0 ± 0.5	61.5
33	CGAGAGTCTGTAATAGCCGATGC	0.25	0.031	3.0 ± 0.2	2.0 ± 0.4	10.6 ± 0.2	63.0
34	GCCTCACATAACTGGAGAAACCT	0.08	0.17	1.67 ± 0.04	4.83 ± 0.06	10.8 ± 0.4	61.5
35	GGCTGTCAATTTATCAGGGAGGC	0.14	0.044	3.22 ± 0.03	2.04 ± 0.04	28.3 ± 0.9	63.0
36	TTCGCTGATTGTAGTGTTGCACA	0.29	−0.44	3.22 ± 0.02	1.6 ± 0.1	0.773 ± 0.007	65.0
37	ATGGGAACCTAAAAGTGTGGCTA	−0.53	0.14	2.24 ± 0.07	2.0 ± 0.5	1.96 ± 0.03	63.5
38	GCATTGAGGTATTGTTGCTCCCA	−0.048	−0.37	1.79 ± 0.03	1.2 ± 0.4	30 ± 1	62.5
39	CCATCAGGAATGACACACACAAA	−1.2	−0.037	2.1 ± 0.2	2.6 ± 0.1	14.7 ± 0.4	61.0
40	ATGCACCGGTAATATTCCTCTGC	−0.44	−1.0	2.5 ± 0.1	3.2 ± 0.2	0.96 ± 0.02*	64.0
41	CGCAGGAATTAACATGATGAGCG	−1.0	−1.0	2.42 ± 0.07	2.1 ± 0.4	1.07 ± 0.02*	62.0
42	GAAACACTGGATACCTGTGGGAC	−1.9	−0.49	4.2 ± 0.4	3.2 ± 0.1	0.342 ± 0.002*	63.0
43	GGGATAGAACTCACGTACTCCCC	−1.2	−1.6	2.55 ± 0.08	4.5 ± 0.3	0.146 ± 0.003*	62.5
44	GGGATCAGTTGTACACTCCCTAG	−1.3	−1.5	4.3 ± 0.2	2.5 ± 0.4	0.585 ± 0.008*	63.5
45	ATGCGTAACACTCCGTATTGCAT	−1.7	−2.0	2.81 ± 0.09	4.5 ± 0.4	0.103 ± 0.001*	65.0
46	GGTCGAAACGTTATATTAACGCG	−2.5	−3.0	8.2 ± 0.2	12.1 ± 0.3	1.93 ± 0.02	64.5

[a]Predicted standard Gibbs free energy change at 25°C of the most stable self-folded structure.
[b]$\Delta F^* = \Delta F/10^2$, where ΔF is the fluorescence intensity change at 25°C obtained by the ssDNA melting experiment.
*Determined by linear regression.

positive ΔG° secondary structure. Here, we derived a model describing how these positive ΔG° secondary structures affect hybridization kinetics, and the model enabled us to calculate hybridization rate constants from base sequences that agreed well with the experimental hybridization rate constants.

MATERIALS AND METHODS

DNA oligonucleotides

A total of 47 pairs of complementary DNA sequences were designed. We denoted one strand in the pair A and the other B. Sequences of the A strands are shown in Table 1, where they are written in the 5′-to-3′ direction. The DNA oligonucleotide sequences used in this study were based on those described by Gotoh *et al.* (29) and were designed *in silico* (i) to contain 23 nucleotides, (ii) to have a similar melting temperature, (iii) to have neither stable misnucleation nor mishybridization, and (iv) to prevent the formation of very stable secondary structures.

Melting temperatures were calculated according to the work of SantaLucia *et al.* (13). Sequences were designed to have melting temperatures of 63.0 ± 2.0°C under conditions of $[Na^+] = 0.195$ M and $[Mg^{2+}] = 0$ M.

The stability of misnucleation was calculated, and the result indicated that five or more unwanted successive base-pairs rarely formed. In addition, the calculations for strand A (or B) using UNAFold (30) indicated that over 99% of A (or B) existed as monomers rather than dimers (AA or BB) under our experimental conditions (25°C, 50 nM single-stranded DNA (ssDNA), $[Na^+] = 0.195$ M, and $[Mg^{2+}] = 0$ M). Therefore, effects of misnucleation and mishybridization were negligible, and we confined this study to intramolecular secondary structures.

Secondary structure prediction of DNA oligonucleotides was performed using UNAFold under our experimental conditions (25°C, $[Na^+] = 0.195$ M, and $[Mg^{2+}] = 0$ M). Additionally, 'no isolated base pairs' and 'no dangle' options were employed, according to Mathews *et al.* (31) and Zhang *et al.* (10), respectively. The probabilities of ssDNA intramolecular base pair formation were calculated using the hybrid2.pl program in UNAFold. The predicted ΔG° values of the secondary structures ranged from −3.0 to 2.2 kcal/mol (Table 1). This range included both previously investigated and unexplored range values. Gao *et al.* (17) reported the effects of secondary structures having negative ΔG° values on DNA hybridization kinetics, and the ΔG^0 values of these secondary structures were −4.4 and −1.7 kcal/mol under our experimental conditions.

All DNA oligonucleotides were commercially synthesized, HPLC purified (SIGMA-Genosys, Hokkaido, Japan), and stored in 1× TE buffer (10 mM Tris–HCl, 1 mM EDTA, pH 8.0) at −20 °C until use.

Thermodynamic measurements

Melting curves of ssDNA and double-stranded DNA (dsDNA) were recorded in the presence of 0.5× SYBR® Green I fluorescent dye (Lonza, Basel, Switzerland) using a CFX96 real-time PCR detection system (Bio-Rad Laboratories, Inc., Hercules, CA, USA). The excitation wavelength was 494 nm, and emission wavelength was 521 nm (optimal fluorescence signal for SYBR® Green I). A total reaction volume of 50 μl and DNA concentrations of 50 nM were used in the experiments. The buffer solution was 1× saline-sodium citrate (SSC) (150 mM NaCl, 15 mM sodium citrate). The reaction mixtures were cooled from 95°C to 15°C at a rate of 0.5°C/min, and subsequently heated to 95°C at the same rate. Fluorescence intensity changes were recorded every 1 min. The melting temperatures for DNA sequences (Table 1) were determined from peaks in the differential melting curve.

Kinetic measurements

An RX-2000 stopped-flow instrument (Applied Photophysics, Surrey, UK) was used to determine the rate of DNA hybridization for the various sequences. A circulating water bath regulated the temperature of the working solutions, which were held in two separate syringes. Each syringe contained a complementary DNA strand solution of equal DNA strand concentrations (50 nM) that was allowed to equilibrate to the indicated temperature before the reaction. The buffer solution was 1× SSC. PicoGreen® fluorescent dye (Invitrogen, Carlsbad, CA, USA) (32,33), a dye for quantitating dsDNA in the presence of ssDNA, was used to observe duplex formation. The syringe drive delivered equal volumes (0.5 ml) of each solution into the reaction chamber through a rapid mixing chamber, with a dead-time of 8 ms. After the solution was inside the reaction chamber, the fluorescence wavelength at 523 nm (with an excitation wavelength of 502 nm) was measured every 0.5 or 1 s, depending on the total time of the experiment, until equilibrium was reached using a fluorescence spectrophotometer LS 55 (Perkin Elmer, Waltham, MA, USA). The total reaction time was 1800–86 400 s. For each duplex forming reaction, at least three injections were performed.

The PicoGreen® intercalating dye bound quickly enough to monitor hybridization (less than 0.5 s, see Supplementary Figure S1). The dye concentration recommended by the manufacturer was used, and the fluorescence intensity was proportional to the dsDNA concentration under our experimental conditions (Supplementary Figure S2). Additionally, we confirmed that the hybridization rates obtained by this method agreed well with those obtained by an absorbance method (Supplementary Figure S3). In this fluorescence method, hybridization could be monitored with DNA concentrations lower than those used in the absorbance method, thus allowing for (i) slower hybridization, such that we could measure hybridization kinetics with a higher time resolution and (ii) lower costs for DNA synthesis, which further enabled us to obtain hybridization data for more types of DNA sequences than previous studies.

The normalized fluorescence intensity was obtained in such a way that one normalized unit (n.u.) of intensity corresponded to the average of the final 200 data points of fluorescence intensity. A fluorescence intensity of 0 n.u. corresponded to the minimum fluorescence data point of each trace, and $t = 0$ also corresponded to this point.

Analysis of kinetic data

DNA hybridization rate constants were determined by linear and nonlinear second-order fitting of the fluorescence data, according to Gao *et al.* (17). Hybridization of two complementary DNA strands was modeled using the simple irreversible second order process: $A + B \xrightarrow{k} AB$. A is a ssDNA strand, B is the complement of A, and AB is the perfect duplex composed of A and B. The concentrations of A, B and AB were designated by C_A, C_B and C_{AB}, respectively. The second-order rate constant for AB duplex formation was notated as k. Initially at time $t = 0$, $C_A = C_{A0}$, $C_B = C_{B0}$ and $C_{AB} = 0$. When $t > 0$, $C_A = (C_{A0} - C_{AB})$, and $C_B = (C_{B0} - C_{AB})$. Hybridization of equal molar A and B strands ($C_A = C_B = C$ and $C_{A0} = C_{B0} = C_0$) can be described by second-order reaction kinetics:

$$\frac{1}{C_0 - C_{AB}} - \frac{1}{C_0} = kt. \quad (1)$$

The observed fluorescence intensity at time t, $F(t)$, and the maximal fluorescence intensity, F_∞, should be proportional to C_{AB} and C_0, respectively. At time $t = 0$, $F(0) = 0$. Substi-

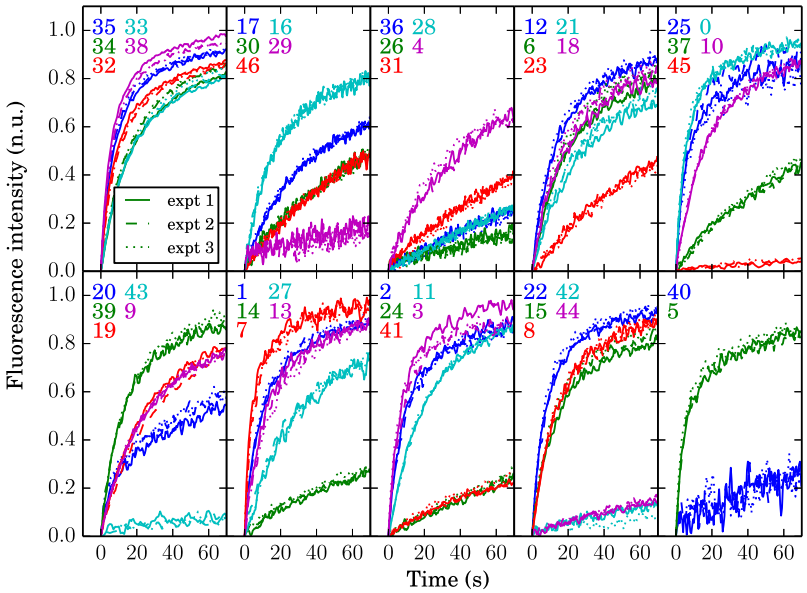

Figure 1. Hybridization kinetics of 47 DNA sequences. Two complementary DNA strands at 50 nM each were rapidly mixed at 25°C in 1× SSC buffer with PicoGreen®. Colors indicate specific sequences and the sequence numbers are shown in the upper left of each panel. Time courses for the initial 70 seconds of three independent experiments are shown.

tuting $F(t)$ and F_∞ into Equation 1 yields the equation:

$$\frac{F_\infty}{F_\infty - F(t)} - 1 = C_0 kt. \quad (2)$$

Here, we describe a plot for the left hand side of Equation 2 versus time as a second-order rate plot. Then, solving for $F(t)$ from Equation (2) yields the following:

$$F(t) = \frac{F_\infty C_0 kt}{1 + C_0 kt}. \quad (3)$$

The rate constant k was determined by linear fitting (Equation 2) or nonlinear fitting (Equation 3) to the fluorescence data for three independent experiments, using SciPy (available at http://www.scipy.org/). In the former fitting, k was the adjustable fitting parameter. The maximal fluorescence intensity F_∞ was constant and determined by the average of the final 200 fluorescence intensity data points. In the latter fitting, fitting of the data up to 80% hybridization were performed with both k and F_∞ as the adjustable fitting parameters. The hybridization rate constants obtained were denoted as k_{app}.

RESULTS

DNA hybridization kinetics

Oligonucleotide hybridization kinetics was determined using a stopped-flow apparatus with fluorescence spectroscopy. Figure 1 shows DNA hybridization kinetic data obtained at 25°C for 47 DNA sequences. Of the 47 DNA sequences, 32 sequences were predicted to have only positive ΔG° secondary structures. The other 15 sequences had negative ΔG° secondary structures for either or both strands, and they were studied for comparison with previous reports on the effects of stable (negative ΔG°) secondary structures on hybridization kinetics. The total number of sequences was much higher than that of previous hybridization kinetic studies (e.g. three sequences in Gao *et al.* (17)). For every sequence, hybridization was measured three times (Figure 1, experiments 1–3), and the obtained kinetic traces were highly reproducible. Only results from the initial 70 seconds are displayed, but the reaction was measured until equilibrium was reached, when the fluorescence is unity. We found that the hybridization rate was strongly dependent on the sequence. For example, sequence no. 35 (blue traces in the first panel) formed 90% of duplexes within 60 s, while sequence no. 29 (purple traces in the second panel) formed only 20%.

In order to test whether the observed oligonucleotide hybridization kinetics was second-order, traditional second-order rate plots of hybridization kinetics for all 47 DNA sequences were constructed (Supplementary Figure S4), and those of typical sequences are shown in Figure 2. Figure 2A–C are the plots for sequences whose hybridization kinetics were able to be fit with a straight line (Equation 2), and panels A-C correspond to data from sequences showing relatively fast, medium, and slow hybridization, respectively. Hybridization kinetics for 40 of the total 47 sequences were able to be fit with a straight line. Thus, their hybridization obeyed second-order kinetics. The resulting hybridization rate constants for the 40 sequences are shown in Table 1. The rate constants varied by two orders of magnitude. For 31 of the 40 sequences, the ΔG° value of the most stable ssDNA secondary structure was positive for both strands. Six sequences had slightly negative ΔG° (e.g. −0.53 kcal/mol) secondary structures for either of the two complementary strands. The other three had negative ΔG° values for both strands (Table 1).

On the other hand, for the other seven of 47 sequences, nos. 20, 40, 41, 42, 43, 44 and 45, their kinetic traces could not be fit to a straight line and curved slightly upward (Fig-

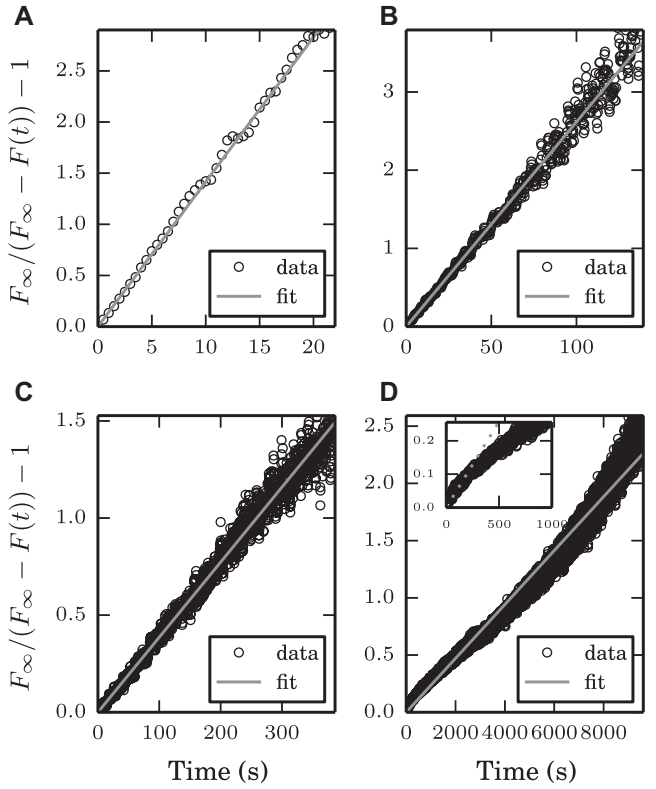

Figure 2. Second-order rate plots of DNA hybridization kinetics. (**A**–**C**) The data from typical sequences with hybridization obeying second-order kinetics. The sequences are (A) no. 35, (B) no. 17 and (C) no. 36. Data up to 80% hybridization are shown. A gray line is the best fit for the data from three independent experiments; data from one experiment is shown here. (**D**) The data from a typical sequence (no. 45) for which hybridization could not be described using second-order reaction kinetics. The inset contains a plot of the data for the initial 1000 s. The dotted line is fit to the initial linear region of data (i.e. up to 250 s) by linear regression using Equation (2).

ure 2D and Supplementary Figure S4). This kind of kinetic trace is similar to that obtained when first-order reactions are plotted with a second-order rate plot. In addition, their hybridizations were relatively slow. They completed 80% duplex formation in $\sim 10^3$ seconds, whereas other sequences took $\sim 10^2$ s. The predicted ΔG° values for these seven sequences were negative for both of the complementary strands, except for sequence no. 20.

In order to obtain second-order rate constants for the seven sequences, we applied the procedure described by Gao *et al.* (17), and performed a linear fit of the initial data points to Equation 2. The inset in Figure 2D shows the initial fluorescence data points of sequence no. 45. The kinetic trace initially increased linearly, but then it curved downward after ~200 s. Only data from no. 45 is displayed here, but this trend was also observed for the other six sequences (Supplementary Figure S5). Gao *et al.* observed this trend using UV absorbance spectroscopy, and they proposed that the first linear kinetic regime corresponds to the nucleation process. Thus, second-order rate constants for nucleation of the seven sequences were obtained by linear fitting, and the results are shown in Table 1 with asterisks. These values were used as the k_{app} for each of the seven sequences.

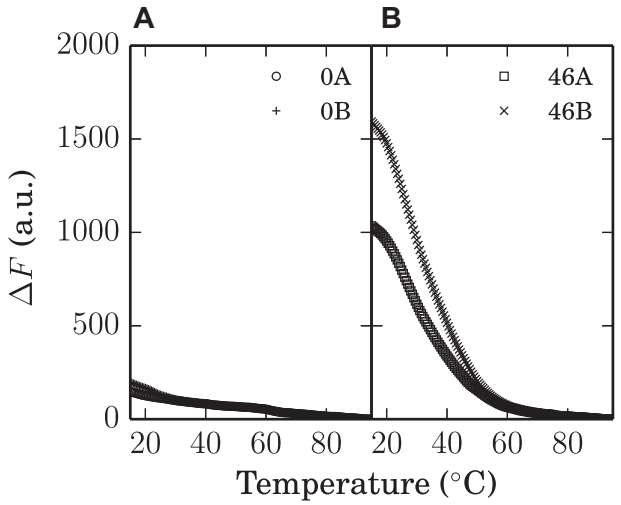

Figure 3. Melting curves of ssDNA for typical DNA sequences monitored by fluorescence spectroscopy. (**A**) Thermal melting of two complementary ssDNA strands (0A and 0B) for a sequence with no known negative ΔG° secondary structure. The sequence is shown in Table 1 (sequence no. 0). Samples of 50 nM ssDNA in 1× SSC and 0.5× SYBR® Green I were heated at a ramp rate of 0.5°C/min. (**B**) Thermal melting of two complementary ssDNA, as in (A), but for a sequence having negative ΔG° ssDNA secondary structures (sequence no. 46).

Melting curves

Melting curves of ssDNA and dsDNA were recorded by the fluorescence method. For dsDNA, melting temperatures obtained from these curves are listed in Table 1. Their melting temperatures fell within the narrow temperature range of 63.5 ± 2.5°C (Table 1). This result ruled out effects of duplex stability on the hybridization kinetics measured in this study as shown later. The average T_m was higher than the predicted value by 0.5°C. This would be because an intercalating dye, SYBR® Green I, increases the thermo-stability of sequences. Actually, our calculation, obtained following the methods of Mcghee *et al.* (34) indicated that an approximate 1°C increment in the T_m value was due to dye intercalation. Therefore, the effect of dye intercalation on stability of dsDNA is not substantial in this case.

For ssDNA melting, typical melting curves are shown in Figure 3. Sequences predicted to have only positive ΔG° secondary structures showed a small fluorescence intensity change, ΔF, compared to the change in dsDNA (Figure 3A). In contrast, sequences having negative ΔG° secondary structures showed relatively large ΔF values (Figure 3B). The fluorescence intensity from ssDNA increases as the number of intramolecular base pairs increases. Therefore, negative ΔG° sequences formed a greater number of intramolecular base pairs than positive ΔG° sequences. Thus, the stability of secondary structures (which increases with the number of existing base pairs) for each sequence qualitatively agreed with the prediction using UNAFold. Quantitatively, in a plot with data from all sequences (Supplementary Figure S6), we observed a positive correlation between the change in fluorescence intensity with ssDNA melting and the predicted intramolecular base pair number. The ΔF values at 25°C are shown in Table 1 as ΔF^*.

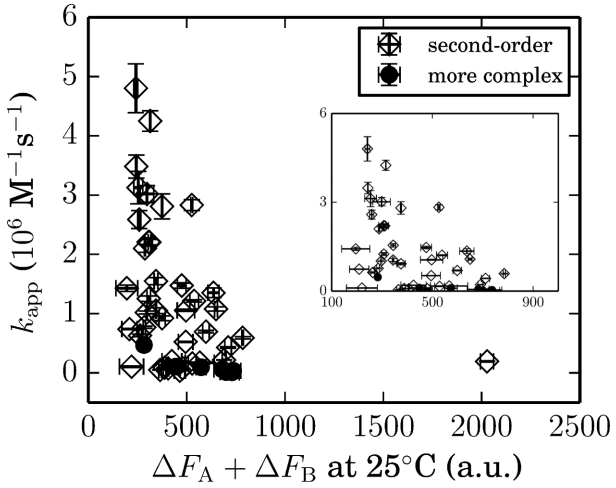

Figure 4. A plot of k_{app} versus $\Delta F_A + \Delta F_B$ at 25°C obtained from the ssDNA melting experiments. Open diamonds correspond to sequences showing second-order reaction kinetics (nos. 0–19 and nos. 21–39, 46). Filled circles correspond to sequences showing more complex reaction kinetics (no. 20 and nos. 40-45; Their k_{app} values were determined by linear regression). Vertical error bars correspond to standard deviations calculated from three independent experiments. Horizontal error bars were calculated from duplicate experiments. The ΔF values for each single strand (shown in Table 1 as ΔF^*) were summed to obatin the value plotted ($\Delta F_A + \Delta F_B$). The inset contains a plot of the data ranged from 100 to 1000 of $\Delta F_A + \Delta F_B$.

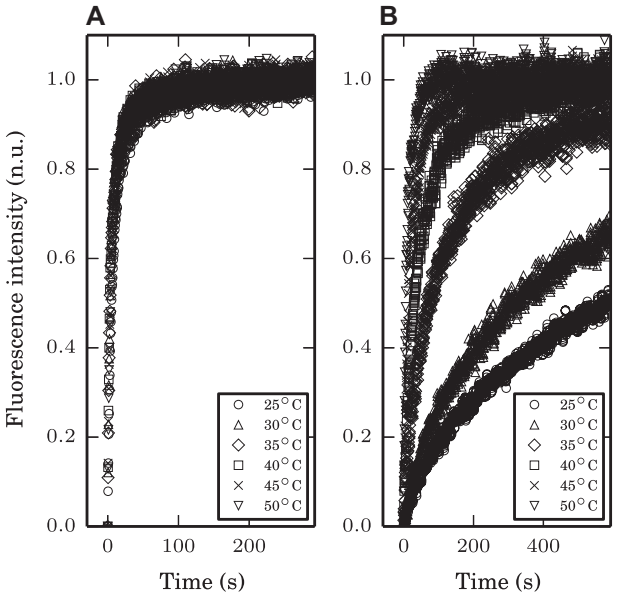

Figure 5. Hybridization kinetics at 25, 30, 35, 40, 45 and 50°C. (**A**) Kinetic data from sequence no. 0., which only has the positive ΔG° secondary structure. Hybridization kinetics was measured three times (one of them is plotted here) for each temperature. (**B**) The kinetic data of sequence no. 44, which has some negative ΔG° secondary structures.

Hybridization rates and secondary structures

We observed that the upperbound of hybridization rate decreased with an increase in probability of base pairing in ssDNA. Figure 4 displays this decrease with a plot of the measured hybridization rate constants k_{app} versus the sum of ΔF for ssDNA pairs at 25°C ($\Delta F_A + \Delta F_B$). As the $\Delta F_A + \Delta F_B$ value increased, the upper limit of the observed hybridization rate constant decreased. This trend was also observed in a plot of k_{app} versus the number of predicted base pairs in ssDNA (Supplementary Figure S7). In addition, we confirmed that a minor difference in duplex stability did not affect the former trend (i.e. a decrease in the upper limit of the hybridization rate constant with the value $\Delta F_A + \Delta F_B$) (Supplementary Figure S8).

Temperature dependence and activation energy of DNA hybridization

To study the temperature dependence of hybridization kinetics, time courses of hybridization at several different temperatures were also determined for some sequences. Figure 5 shows the kinetic data from two typical sequences; one shows second-order hybridization (Figure 5A), and the other shows more complex hybridization (Figure 5B). (For other sequences, see Supplementary Figure S9.) The hybridization rate of the former sequence changed little in the temperature range compared with that of the latter sequence. This is due to a difference in the stability of secondary structures, and a similar trend was observed in a comparison between the hybridization of unstructured coils and hybridization with stable secondary structures (18,35,36). Thus, hybridization with a positive ΔG° secondary structure showed a similar temperature dependence as unstructured-coil hybridization.

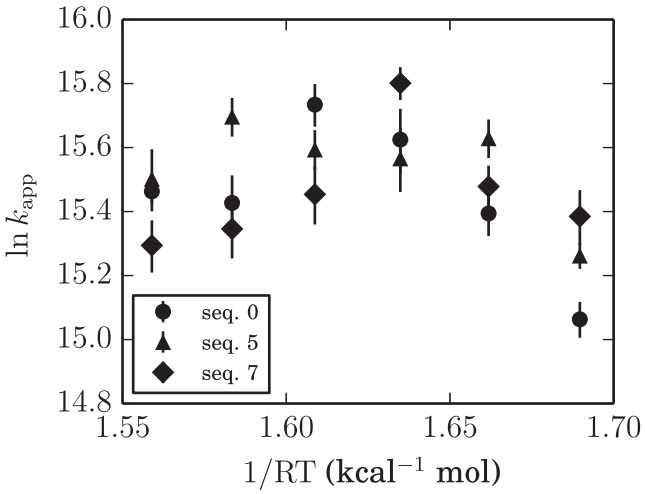

Figure 6. Arrhenius plots for the hybridization rate constants of sequences nos. 0, 5 and 7 determined by non-linear fitting of the data from three independent experiments. Error bars indicate standard deviations of the fitted variable.

For sequences showing second-order hybridization, hybridization rate constants were obtained at 25, 30, 35, 40, 45 and 50°C, and plotted in Figure 6. The temperature dependence of the hybridization rate constants exhibited non-Arrhenius behavior, and apparent activation energies of hybridization changed from negative at high temperatures to positive at low temperatures. The values of activation energies extracted from the plot are shown in Table 2.

Table 2. Apparent activation energies in the respective temperature ranges

No.	E_a (kcal/mol)[a]	E_a (kcal/mol)[b]
0	11 ± 1	−7 ± 4
5	8 ± 4	0 ± 3
7	8 ± 2	−3 ± 1

[a]Fitting temperature range: 25–35°C.
[b]Fitting temperature range: 40–50°C.

DISCUSSION

Influence of thermodynamically unfavorable secondary structures on DNA hybridization kinetics

In this paper, the influences of thermodynamically unfavorable secondary structures on hybridization kinetics were studied. Thermodynamically unfavorable in this paper, means that the standard Gibbs free energy change ΔG° for the formation of the secondary structure is positive. Of the 47 DNA sequences used in this study, 32 sequences were predicted to have only positive ΔG° secondary structures. Such secondary structures and their influence on hybridization kinetics were systematically studied here. The other 15 sequences had negative ΔG° secondary structures for either or both strands, and they were studied for comparison with previous reports on the effects of stable (negative ΔG°) secondary structures on hybridization kinetics.

For sequences with positive ΔG° secondary structures, the observed hybridization kinetics differed significantly from sequence to sequence (Figure 1). Despite the large differences in hybridization rates, all of the hybridization obeyed second-order reaction kinetics, except for sequence no. 20 (Figure 2, Figure S4). This result means that the hybridization of these sequences is a bimolecular reaction. The determined bimolecular rate constants varied two orders of magnitude among the sequences (Table 1).

In addition, the temperature dependence of the hybridization rates for sequences with positive ΔG° secondary structures showed non-Arrhenius behavior (Figure 6). The same behavior has been found in the hybridization of nucleic acid sequences with no secondary structure (7). To understand this behavior, the following explanation based on the nucleation-limited nucleation-zipper model for the hybridization has been applied: at low temperatures, a diffusion-controlled nucleation process is the origin of positive activation energy E_a, and the negative E_a at high temperature is due to the existence of metastable intermediates in the nucleation process. This explanation should apply to the hybridization of sequences with positive ΔG° secondary structures and, therefore, their hybridization must be nucleation limited.

The upperbound of hybridization rate of sequences with positive ΔG° secondary structures decreased with $\Delta F_A + \Delta F_B$ (Figure 4). The $\Delta F_A + \Delta F_B$ value increases as the number of intramolecular base pairs in ssDNA. Therefore, the upperbound of hybridization rate decreases with the number of intramolecular base pairs, even if the secondary structures formed by the intramolecular base pairing show positive ΔG° values. This indicates that the positive ΔG° secondary structures prevent the nucleation process in hybridization, rather than such thermodynamically unfavorable secondary structures being too unstable to have any substantial effects on hybridization kinetics, as previously believed. This would not be surprising when taking into consideration that such positive ΔG° secondary structures exist at almost the same concentration as the unstructured coil when the absolute value of ΔG° is very small.

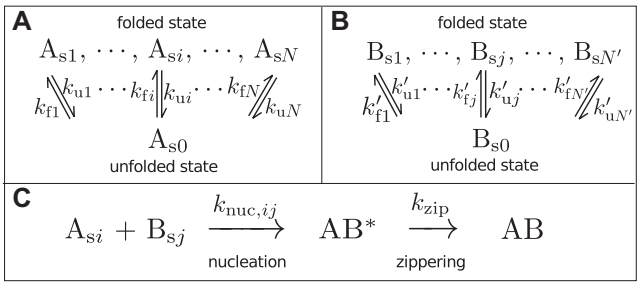

Figure 7. A schematic of hybridization with positive ΔG° secondary structures. (**A**) An A strand has an unfolded state and N folded states (positive ΔG° secondary structures). Transitions between these states occur with state-dependent rate constants. (**B**) Transitions between states for a B strand. (**C**) Hybridization is divided into two processes of nucleation and zippering. Nucleation occurs between a pair of A and B in any strand states. The nucleation rate constant depends on the pair, because the number of nucleation sites differs from state to state. The subsequent zippering is much faster than the nucleation, and the dependence of the rate constant on zippering of the pair is not considered substantial.

For some sequences with negative ΔG° secondary structures, we observed non-second-order hybridization. The second-order rate plots for their hybridization showed the same trend as the results reported in (17) (Figure 2). In the case of negative ΔG° secondary structures, after the nucleation process, there is a large free energy barrier with the destruction of secondary structures (17,18). This energy barrier makes the hybridization kinetics more complex.

Hybridization model with thermodynamically unfavorable secondary structures

Here, we derive a reaction model for hybridization with positive ΔG° secondary structures from our experimental observations. Figure 7 shows a schematic of our model, which is an improved nucleation-zipper model taking into account the influence of positive ΔG° secondary structures. An A (or B) strand has $N + 1$ (or $N' + 1$) conformational states: a strand in an unfolded state A_{s0} (or B_{s0}) and those in N (or N') folded states with positive ΔG° secondary structures, $A_{si} (1 \leq i \leq N)$ (or $B_{sj} (1 \leq j \leq N')$) (Figure 7A and B). Here we note that not only the optimal (most stable) secondary structure but also suboptimals (semi-stable secondary structures) are considered in our model. Based on the traditional nucleation-zipper model for oligonucleotide hybridization (9), a nucleus composed of a small number of successive base-pairs forms first (nucleation process), and subsequently, the double helix can zip up (zippering process). Nucleation can occur between a pair of A and B in any strand states, followed by zippering (Figure 7C). The un-nucleation rate ($AB^* \rightarrow A + B$) was ignored because it is much smaller than k_{nuc} under our experimental conditions (not at a temperature of negative E_a).

In addition, the following conditions should be satisfied because of our experimental observation that the hybridization was a second-order reaction: (i) the zippering rate (k_{zip}) was much larger than the nucleation rate (k_{nuc}) and (ii) transitions between the unfolded state and folded states were much faster than the nucleation rate (i.e. k_f, $k_u \gg k_{nuc}$). Therefore, the observed decrease in the upperbound of hybridization rate with $\Delta F_A + \Delta F_B$ can be attributed to the decrease in k_{nuc} probably because of a reduction in nucleation sites caused by stem (base-paired) and loop regions, which are less accessible than coil regions.

Hybridization rate calculation from base sequence

To quantitatively validate our model, here we calculated the hybridization rate, k_{calc}, from the base sequence, and compared it with the experimental hybridization rate, k_{app}. The value of k_{calc} should be proportional to (i) the number of nucleation sites in a strand, and (ii) the nucleation capability of each nucleation site.

The former can be determined by the predicted secondary structure. Considering the concentration distribution for various secondary structures formed by an ssDNA, a nucleation site density, ρ, was adopted (for derivation of the equation, see Supporting Information; Appendix S1). The ρ value represents the number of nucleation sites per the maximum number of nucleation sites in a strand, which is unity when the strand forms no secondary structures (unstructured coil). The value of ρ was calculated for both the A and B strands, multiplied:

$$\rho^{AB} = \rho_A \rho_B = \sum_{i=0}^{N} \frac{C_{A_{si}}}{C_A} \frac{n_{A_{si}}}{n_{A_{s0}}} \sum_{j=0}^{N'} \frac{C_{B_{sj}}}{C_B} \frac{n_{B_{sj}}}{n_{B_{s0}}}, \quad (4)$$

where C denotes the concentration of strands, and n represents the number of nucleation sites. The subscript si (or sj) denotes an ith (or jth) conformational state of the strand. The 0th state is the unfolded state, and the first state is the optimal (most stable) folded state. Suboptimal folded states with ΔG° values less than +1 kcal/mol above the ΔG° of the optimal folded state were considered. Here, $C_A = \sum_{i=0}^{N} C_{A_{si}}$, $C_B = \sum_{j=0}^{N'} C_{B_{sj}}$, $C_{A_{si}}/C_{A_{s0}} = \exp(-\Delta G^\circ_{A_{si}}/RT)$, and $C_{B_{sj}}/C_{B_{s0}} = \exp(-\Delta G^\circ_{B_{sj}}/RT)$, where $\Delta G^\circ_{A_{si}}$ (or $\Delta G^\circ_{B_{sj}}$) is the standard Gibbs free energy change for formation of the ith (or jth) strand state. R is the gas constant and T is the absolute temperature.

The nucleation capability of each nucleation site can be determined mainly by three factors: the steric hindrance, flexibility, and base sequence of each nucleation site. Figure 8 is a schematic view of these factors. For steric hindrance, parameter δ_{sth} was adopted. Nucleation sites located at stems, and also around stem regions, can be inaccessible due to steric hindrance. In such nucleation sites, $\delta_{sth} = 0$; otherwise, $\delta_{sth} = 1.0$. For flexibility, bases involved in loops, and also stems, are less flexible than bases in coil regions. This effect was represented by parameter δ_{flx}, which is unity when the nucleation site is in coil regions. For the base sequence, parameter δ_{seq} was adopted. The value of δ_{seq} represents the difference in the nucleation capability among

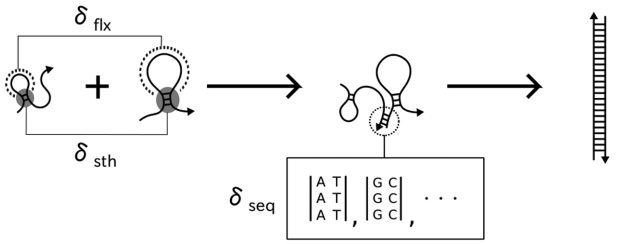

Figure 8. A schematic view of three parameters (δ_{sth}, δ_{flx} and δ_{seq}) determining the nucleation capability. Triangle-head arrows represent ssDNA strands. Lines connecting the arrows represent base pairs. In gray regions, nucleation is prevented by steric hindrance, whose effect is represented by δ_{sth}. Dotted lines indicate loops in which strand flexibility decreases, whose effect is represented by δ_{flx}. The dotted circle indicates a nucleus, which can be composed of different base sequences and whose effect is represented by δ_{seq}.

base sequences at a nucleation site. To sum up, the nucleation capability, δ, of a nucleation site is represented by the following:

$$\delta = \delta_{sth}\delta_{flx}\delta_{seq}. \quad (5)$$

Considering the nucleation capability, an effective number of nucleation sites, n^*, of a secondary structure formed by a 23-nt strand is calculated by the equation: $n^* = \sum_{m=1}^{23-L_{nuc}+1} \delta_m$, where L_{nuc} is the number of bases composing a nucleation site, and δ_m represents δ of the mth nucleation site in a strand. Substituting n^* for n in Equation (4) yields an equation for evaluating the nucleation rate:

$$k_{calc} = k_0 \sum_{i=0}^{N} \frac{C_{A_{si}}}{C_A} \frac{n^*_{A_{si}}}{n_{A_{s0}}} \sum_{j=0}^{N'} \frac{C_{B_{sj}}}{C_B} \frac{n^*_{B_{sj}}}{n_{B_{s0}}}, \quad (6)$$

where k_0 is the rate constant of hybridization between unfolded strands with $\delta_{seq} = 1$ for all base sequences.

As a first approximation, we assumed $\delta_{seq} = 1$ for all base sequences. The k_{calc} value calculated with an approximation of $\delta_{seq} = 1$ is denoted as k'_{calc}. The values of δ_{sth} and δ_{flx} were determined to maximize the correlation coefficient between k_{app} and k'_{calc}. As a result, for nucleation sites located in stem regions and within two bases from a stem region, $\delta_{sth} = 0$, otherwise, $\delta_{sth} = 1.0$. Also, $\delta_{flx} = 1.0$ for all nucleation sites with $\delta_{sth} = 1.0$ even though they are in loop regions. These results were obtained with the condition $L_{nuc} = 3$ (Supplementary Figure S10a). In the case of $L_{nuc} = 4$, the similar trend was observed (Supplementary Figure S10B). Thus, we used the above values of δ_{sth} and δ_{flx} with $L_{nuc} = 3$. Figure 9A shows a plot of k_{app} versus k'_{calc}. The upper bound (dashed line) and the lower bound (dotted line) of k_{app} increased with k'_{calc}. However, the relationship between them is not completely proportional. Even though the sequences have almost the same k'_{calc} value, there is a large difference in the hybridization rates for the different sequences. For example, the sequences with k'_{calc}/k_0 values of about 0.8 have rate constants that vary by at least an order of magnitude.

Then, we parameterized δ_{seq} for every base triplet. The values of δ_{seq} were determined to maximize the correlation coefficient between k_{app} and k_{calc}. As a result, we obtained a clear proportional relationship between them (Fig-

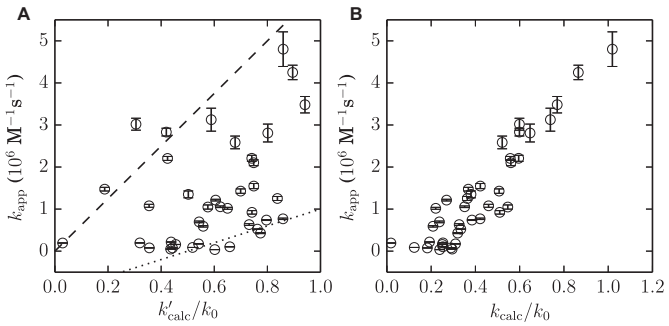

Figure 9. A comparison of the observed hybridization rate, k_{app}, and the calculated hybridization rate. (**A**) The value of k'_{calc}/k_0 calculated under the assumption of $\delta_{seq} = 1$ for all base sequences. Dashed and dotted line are drawn to guide the eye. The dashed and dotted line have slopes of 6.3 and 2.0, respectively. (**B**) The k_{calc}/k_0 value was determined with δ_{seq} values listed in Table 3. The correlation coefficient is 0.92.

Table 3. List of δ_{seq} parameters for base triplets

Sequence	δ_{seq}[a]	Sequence	δ_{seq}[a]
AGG/CCT	3.5 ± 0.6	GCG/CGC	0.7 ± 0.3
GTG/CAC	2.2 ± 0.4	AAA/TTT	0.5 ± 0.1
GAG/CTC	2.1 ± 0.4	TAG/CTA	0.4 ± 0.2
TTG/CAA	2.3 ± 0.5	CGG/CCG	0.2 ± 0.3
ATC/GAT	1.7 ± 0.4	CAG/CTG	0.1 ± 0.2
GGC/GCC	1.7 ± 0.3	AGA/TCT	0.1 ± 0.1
AAT/ATT	1.6 ± 0.3	GGG/CCC	0.3 ± 0.2
ATA/TAT	1.6 ± 0.3	AAC/GTT	0.0 ± 0.2
TGG/CCA	1.7 ± 0.4	ATG/CAT	0.0 ± 0.1
ACA/TGT	1.8 ± 0.3	AGT/ACT	0.5 ± 0.2
ACC/GGT	1.5 ± 0.4	AGC/GCT	0.00 ± 0.09
TCC/GGA	1.2 ± 0.3	ACG/CGT	0.00 ± 0.03
TCG/CGA	1.1 ± 0.3	TAA/TTA	0.0 ± 0.1
TAC/GTA	0.9 ± 0.2	TTC/GAA	0.00 ± 0.05
TGC/GCA	0.9 ± 0.3	TGA/TCA	0.0 ± 0.2
AAG/CTT	0.4 ± 0.2	GAC/GTC	0.0 ± 0.2

[a]The uncertainties of determined δ_{seq} parameters were evaluated using Monte Carlo simulations (see Supporting Information; Appendix S2).

ure 9B). Determinations were made using Scipy (see Supporting Information; Appendix S2) with a constraint that triplets complimentary each other have the same δ_{seq} value. The obtained δ_{seq} values are shown in Table 3. All triplets were found at least 16 times in the sequences studied (Table S1), thus over-fitting did not occur in this case. In addition, to evaluate the adequacy of δ_{seq} values, samples were randomly divided into two groups: one for the determination of δ_{seq} values (learning samples), and the other for testing the utility of the k_{calc} calculation (test samples). The results are shown in Supplementary Table S2. The correlation of k_{app} and k_{calc} for test samples (r_{test}) improved in the result of δ_{seq} determination, which did not depend on the number of learning samples (Δr_{test} was positive for all cases). This shows that the obtained δ_{seq} values were not artifacts, but were related to kinetic properties of sequence-dependent nucleus formation. The value of r_{test} increased with the number of learning samples, so we used δ_{seq} values determined from all 40 samples (Table 3) in the following discussion.

In order to gain insights into the mechanisms underlying the sequence dependence of nucleation capability (δ_{seq}), we first compared δ_{seq} values with nucleus stability (ΔG°_{nuc}) calculated from the NN parameter (13), but no clear correlation was observed (Supplementary Figure S11a). Also, the δ_{seq} values were compared with enthalpy and entropy change (ΔH°_{nuc} and ΔS°_{nuc}, respectively), for formation of a nucleus duplex, calculated from the NN parameters, however there was no strong correlation (Supplementary Figure S11b-c). Although the sequence dependence of ssDNA conformations, such as the single-strand base-stacking (38), can be related to the sequence dependence of δ_{seq}, more detailed invesigations such as molecular dynamics simulations would be necessary to elucidate the underlying mechanisms.

Temperature dependence of the hybridization rate

To evaluate the contribution of positive ΔG° secondary structures to the temperature dependence of the hybridization rate, we calculated the temperature dependence of the value of k_{calc} using UNAFold with the determined δ_{seq} parameters (Supplementary Figure S12). Here we assumed that δ_{seq} values are constant with temperature. The value of k_{calc} gradually increased with temperature, because intramolecular base pairs are less stable at higher temperatures. The increments in k_{calc} of the sequences were within 3–6% in the temperature range 25–35°C, while k_{app} increased 41–93% in the same temperature range. Thus, the decrement in the positive ΔG° secondary structures corresponded to only 4–15% in the increment of k_{app}. This suggests that, in order to understand the temperature dependence of hybridization rate, δ_{seq} values need to be further studied as a function of temperature.

CONCLUSION

We revealed that thermodynamically unfavorable (positive ΔG°) ssDNA secondary structures significantly affect oligonucleotide hybridization kinetics. Previous studies have focused only on stable (negative ΔG°) secondary structures in this context. Our experiments indicated that (i) the hybridization of complementary DNA strands with positive ΔG° secondary structures is nucleation limited, and (ii) the hybridization rate tends to decrease with the stability of positive ΔG° secondary structures. Therefore, influences of the stability of positive ΔG° secondary structures on hybridization kinetics are attributed to a decrease in the nucleation rate. In addition, our hybridization model, with consideration of positive ΔG° secondary structures, allowed a quantitative characterization of the dependence of the hybridization rate on base sequences of nucleation sites. The influence of positive ΔG° secondary structures can be found in various applications utilizing hybridization such as biosensors, PCR, and DNA origami. In such technologies, understanding positive ΔG° secondary structures will enable us to adjust the hybridization rate more precisely. In addition, our observations on DNA hybridization are applicable to RNA hybridization. Therefore, this study provides further insight into the mechanisms of RNA-RNA interactions such as the RNA interference in gene expression.

SUPPLEMENTARY DATA

Supplementary Data are available at NAR Online.

ACKNOWLEDGEMENTS

We thank Yoko Sakai for technical assistance in DNA melting experiments. H.H. acknowledges support from the Japan Society for the Promotion of Science through Program for Leading Graduate Schools (MERIT).

FUNDING

Grant-in-Aid for Scientific Research on Innovative Areas [23119007 to A.S.] from the Ministry of Education, Culture, Sports, Science and Technology, Japan. Funding for open access charge: The University of Tokyo.
Conflict of interest statement. None declared.

REFERENCES

1. Watson,J.D. and Crick,F.H. (1953) Molecular structure of nucleic acids; a structure for deoxyribose nucleic acid. *Nature*, **171**, 737–738.
2. Saiki,R.K., Gelfand,D.H., Stoffel,S., Scharf,S.J., Higuchi,R., Horn,G.T., Mullis,K.B. and Erlich,H.A. (1988) Primer-directed enzymatic amplification of DNA with a thermostable DNA polymerase. *Science*, **239**, 487–491.
3. Wetmur,J.G. (1991) DNA probes: applications of the principles of nucleic acid hybridization. *Crit. Rev. Biochem. Mol. Biol.*, **26**, 227–259.
4. Schena,M., Shalon,D., Davis,R.W. and Brown,P.O. (1995) Quantitative monitoring of gene expression patterns with a complementary DNA microarray. *Science*, **270**, 467–470.
5. Chee,M., Yang,R., Hubbell,E., Berno,A., Huang,X.C., Stern,D., Winkler,J., Lockhart,D.J., Morris,M.S. and Fodor,S.P. (1996) Accessing genetic information with high-density DNA arrays. *Science*, **274**, 610–614.
6. Wetmur,J. and Davidson,N. (1968) Kinetics of renaturation of DNA. *J. Mol. Biol.*, **31**, 349–370.
7. Craig,M.E., Crothers,D.M. and Doty,P. (1971) Relaxation kinetics of dimer formation by self complementary oligonucleotides. *J. Mol. Biol.*, **62**, 383–401.
8. Pörschke,D. and Eigen,M. (1971) Co-operative non-enzymic base recognition III. Kinetics of the helix-coil transition of the oligoribouridylic· oligoriboadenylic acid system and of oligoriboadenylic acid alone at acidic pH. *J. Mol. Biol.*, **62**, 361–381.
9. Bloomfield,V.A., Crothers,D.M. and Tinoco,I. (2000) *Nucleic Acids: Structures, Properties, and Functions*. University Science Books, Sausalito.
10. Zhang,D.Y. and Winfree,E. (2009) Control of DNA strand displacement kinetics using toehold exchange. *J. Am. Chem. Soc.*, **131**, 17303–17314.
11. Rauzan,B., McMichael,E., Cave,R., Sevcik,L.R., Ostrosky,K., Whitman,E., Stegemann,R., Sinclair,A.L., Serra,M.J. and Deckert,A. (2013) Kinetics and thermodynamics of DNA, RNA, and hybrid duplex formation. *Biochemistry*, **52**, 765–772.
12. Sikora,J.R., Rauzan,B., Stegemann,R. and Deckert,A. (2013) Modeling stopped-flow data for nucleic acid duplex formation reactions: The importance of off-path intermediates. *J. Phys. Chem. B*, **117**, 8966–8976.
13. SantaLucia,J. (1998) A unified view of polymer, dumbbell, and oligonucleotide DNA nearest-neighbor thermodynamics. *Proc. Natl. Acad. Sci. U.S.A.*, **95**, 1460–1465.
14. Zuker,M. (2003) Mfold web server for nucleic acid folding and hybridization prediction. *Nucleic Acids Res.*, **31**, 3406–3415.
15. McCaskill,J.S. (1990) The equilibrium partition function and base pair binding probabilities for RNA secondary structure. *Biopolymers*, **29**, 1105–1119.
16. Yin,Y. and Zhao,X. (2011) Kinetics and dynamics of DNA hybridization. *Acc. Chem. Res.*, **44**, 1172–1181.
17. Gao,Y., Wolf,L.K. and Georgiadis,R.M. (2006) Secondary structure effects on DNA hybridization kinetics: a solution versus surface comparison. *Nucleic Acids Res.*, **34**, 3370–3377.
18. Chen,C., Wang,W., Wang,Z., Wei,F. and Zhao,X.S. (2007) Influence of secondary structure on kinetics and reaction mechanism of DNA hybridization. *Nucleic Acids Res.*, **35**, 2875–2884.
19. Sekar,M.M.A., Bloch,W. and St John,P.M. (2005) Comparative study of sequence-dependent hybridization kinetics in solution and on microspheres. *Nucleic Acids Res.*, **33**, 366–375.
20. Mir,K.U. and Southern,E.M. (1999) Determining the influence of structure on hybridization using oligonucleotide arrays. *Nat. Biotechnol.*, **17**, 788–792.
21. Riccelli,P. V, Merante,F., Leung,K.T., Bortolin,S., Zastawny,R.L., Janeczko,R. and Benight,A.S. (2001) Hybridization of single-stranded DNA targets to immobilized complementary DNA probes: comparison of hairpin versus linear capture probes. *Nucleic Acids Res.*, **29**, 996–1004.
22. Kitajima,T., Takinoue,M., Shohda,K. and Suyama,A. (2008) Design of code words for DNA computers and nanostructures with consideration of hybridization kinetics. *Lect. Notes Comput. Sci.*, **4848**, 119–129.
23. Schreck,J.S., Ouldridge,T.E., Romano,F., Šulc,P., Shaw,L.P., Louis,A.A. and Doye,J.P.K. (2015) DNA hairpins destabilize duplexes primarily by promoting melting rather than by inhibiting hybridization. *Nucleic Acids Res.*, **43**, 6181–6190.
24. Genot,A.J., Zhang,D.Y., Bath,J. and Turberfield,A.J. (2011) Remote toehold: a mechanism for flexible control of DNA hybridization kinetics. *J. Am. Chem. Soc.*, **133**, 2177–2182.
25. Seelig,G., Soloveichik,D., Zhang,D.Y. and Winfree,E. (2006) Enzyme-free nucleic acid logic circuits. *Science*, **314**, 1585–1588.
26. Qian,L. and Winfree,E. (2011) Scaling up digital circuit computation with DNA strand displacement cascades. *Science*, **332**, 1196–1201.
27. Sobczak,J.P.J., Martin,T.G., Gerling,T. and Dietz,H. (2012) Rapid folding of DNA into nanoscale shapes at constant temperature. *Science*, **338**, 1458–1461.
28. Myhrvold,C., Dai,M., Silver,P.A. and Yin,P. (2013) Isothermal self-assembly of complex DNA structures under diverse and biocompatible conditions. *Nano Lett.*, **13**, 4242–4248.
29. Gotoh,O., Murakami,Y. and Suyama,A. (2011) Multiplex cDNA quantification method that facilitates the standardization of gene expression data. *Nucleic Acids Res.*, **39**, e70.
30. Markham,N.R. and Zuker,M. (2008) UNAFold: software for nucleic acid folding and hybridization. In: Keith,JM (ed). *Bioinformatics, Volume II. Structure, Function and Applications*. Humana Press, Totowa, pp. 3–31.
31. Mathews,D.H., Sabina,J., Zuker,M. and Turner,D.H. (1999) Expanded sequence dependence of thermodynamic parameters improves prediction of RNA secondary structure. *J. Mol. Biol.*, **288**, 911–940.
32. Singer,V.L., Jones,L.J., Yue,S.T. and Haugland,R.P. (1997) Characterization of PicoGreen reagent and development of a fluorescence-based solution assay for double-stranded DNA quantitation. *Anal. Biochem.*, **249**, 228–238.
33. Dragan,A.I., Casas-Finet,J.R., Bishop,E.S., Strouse,R.J., Schenerman,M.A. and Geddes,C.D. (2010) Characterization of PicoGreen interaction with dsDNA and the origin of its fluorescence enhancement upon binding. *Biophys. J.*, **99**, 3010–3019.
34. McGhee,J. (1976) Theoretical calculations of the helix-coil transition of DNA in the presence of large, cooperatively binding ligands. *Biopolymers*, **15**, 1345–1375.
35. Morrison,L.E. and Stols,L.M. (1993) Sensitive fluorescence-based thermodynamic and kinetic measurements of DNA hybridization in solution. *Biochemistry*, **32**, 3095–3104.
36. Pörschke,D., Uhlenbeck,O.C. and Martin,F.H. (1973) Thermodynamics and kinetics of the helix-coil transition of oligomers containing GC base pairs. *Biopolymers*, **12**, 1313–1335.
37. Seol,Y., Skinner,G., Visscher,K., Buhot,A. and Halperin,A. (2007) Stretching of homopolymeric RNA reveals single-stranded helices and base-stacking. *Phys. Rev. Lett.*, **98**, 158103.
38. Ramprakash,J., Lang,B. and Schwarz,F.P. (2008) Thermodynamics of single strand DNA base stacking. *Biopolymers*, **89**, 969–979.